The Vibrations Induced by Fluid Flow in Plates with Different Poisson's Ratios

Bartłomiej BURLAGA, Tomasz STRĘK

Institute of Applied Mechanics, Poznan University of Technology
ul. Jana Pawła II 24, 60-965 Poznań, Poland
bartlomiej.burlaga@put.poznan.pl
tomasz.strek@put.poznan.pl

Abstract

A fluid interacts with every solid object that is submerged in its flow. In this paper, the dynamic instability of elastic solid is modeled and analyzed based on the benchmark model. It is caused by a continuous stream of vortices (known as von Kármán vortex street). In the presented approach, prerequisites are calculated to meet the necessary conditions for this phenomenon to occur. The main objective of this study is to determine the influence of different Poisson ratios on the intensity of a solid body's deflection. In the first part, governing equations are presented. The following part describes the model domain as well as assumed parameters with chosen values explanation. The third part presents simulation specific information – mesh and applied options. The conclusion and possible real-life applications are preceded by obtained results.

Keywords: auxetic, fluid-structure interaction, finite element method, Poisson's ratio, vibrations

1. Introduction

The main problems in aeroelasticity are divergence, control reversal, and flutter. The last of them is also the most destructive one. There are some well-known examples of design failure due to dynamic instability in fluid flow, with Tacoma Narrows Bridge being one of the biggest. For that reason, this phenomenon is the topic of scientific research for almost 100 years [1]. In such a long period, manufacturing technologies and materials were enhanced or new ones were invented. In current research the behavior of new structures made of new materials in the fluid flow is modeled and analyzed [2-4].

The scientific interest in metamaterials is growing in recent years [3-5]. One group of them are auxetics – materials with negative Poisson's ratio (NPR). They were the subject of scientific investigations carried since 1978. In 1987, Lakes [6] presented the first foam structure that shows this behavior and this process is still under development [7].

The most common auxetic metamaterials are arranged in foams or cellular structures. One of their key property is low density and the ability to dissipate energy. Damping properties of beams with auxetic core were investigated by Strek et. al. [8]. In this study, different loading conditions and parameters were applied. Conclusions implied that materials with a lower value of Poisson's ratio have higher mechanical impedance. The higher damping properties of auxetic foams were proven by Scarpa [9]. In their study, authors compared the damping properties of conventional polyurethane-polyethylene foam to one with a negative Poisson's ratio. The results showed that auxetic foams are good vibration dampers both in low and high frequencies. These conclusions were

confirmed in further work [10-11]. In the first paper, the auxetic structure (anti-tetrachiral) showed higher damping properties than conventional material. Authors of the second papers modeled vibrations of three-dimensional auxetic structures in a wider range of frequencies. The higher values for vibration transmission loss were observed for materials with negative Poisson's ratio, but the specific value depended on characteristic dimensions of a single cell in the structure.

The main objective of this paper is to investigate the influence of different values of Poisson's ratio on material deformations induced by fluid flow. For comparison purposes, the well-known benchmark model was used.

2. Governing equations

In our study, we created two domains that interact with each other. One of them is the Newtonian fluid domain, in which incompressible flow occurs – denoted as Ω_f. The other one is elastic solid – denoted as Ω_s. The following equation defines part of the boundary, where fluid interacts with solid:

$$\Gamma_0 = \overline{\Omega_f} \cap \overline{\Omega_s}. \tag{1}$$

The time is described as $t \in [0, T]$.

2.1. Solid mechanics

As mentioned previously, the solid was treated as an elastic and deformable object. Its state, in a given moment, is defined by displacement u_s with the corresponding velocity field $v_s = \frac{\delta u_s}{\delta t}$. The basic equilibrium equation in $\Omega_s(t)$ is shown as:

$$\rho_s \left(\frac{d^2 u_s}{dt^2}\right) + \rho_s(\nabla v_s)v_s = div(\sigma_s) + \rho_s g. \tag{2}$$

The equation (2) can be rewritten concerning the initial state (or another fixed one) and its form is as follows:

$$\rho_s \left(\frac{d^2 u_s}{dt^2}\right) = div(J\sigma_s F^{-T}) + \rho_s g, \tag{3}$$

where the deformation gradient vector is denoted as $F = I + \nabla u_s$. To fully specify material Cauchy stress tensor σ_s is given by law for hyperelastic material (St. Venant-Kirchoff model formulation) and can be written in form of equation:

$$\sigma_s = \frac{1}{J} F(\lambda_s(rE)I + 2\mu_s E)F^T. \tag{4}$$

The initial (undeformed) structure has density described as ρ_s. The material is defined by Young modulus E and its Poisson's ratio v_s [13,14].

2.2. Fluid mechanics

As stated above, we assumed the fluid to be Newtonian and flow to be incompressible. The state of flow, at any given time, is described by its velocity u_f and pressure fields p_f:

$$\rho_f \frac{du_f}{dt} + \rho_f(\nabla u_f)u_f = div\ \sigma_f,$$
$$div\ \sigma_f = 0. \tag{5}$$

Equation (5) is the general balance equation for this problem in $\Omega_s(t)$. The constitutive equation for the material is given by following equation:

$$\sigma_f = -p_f I + \rho_f v_f(\nabla u_f + \nabla u_f^T). \tag{6}$$

The density of the fluid ρ_f is assumed constant. The dynamic viscosity is denoted as v_f [12-14].

One of the commonly used parameters used to describe the character of the flow is Reynold's number. It is defined as:

$$Re = \frac{l\,u}{v_d}, \tag{7}$$

where l is the characteristic dimension, u is fluid velocity and v_d is kinematic viscosity. In general, the higher the value the more turbulent flow [14].

2.3. Fluid-structure interaction conditions

On the interface between fluid and solid following conditions are required to obtain two-way coupling. In that situation, fluid flow deforms solid and solid changes fluid domain:

$$\sigma_f\,n = \sigma_s\,n\,,$$
$$u_f = v_s\,, \tag{8}$$

where n is the unit vector, normal to the interface $\Gamma_0(t)$. The application of these equations ensures no-slip conditions in flow and balance of forces on the interface [10,12].

The fluid-structure interaction uses arbitrary Lagrangian-Eulerian (*ALE*) finite element method. The Navier-Stokes equations for viscous, incompressible flow might be written in following form:

$$\dot{u} + \nabla \cdot (u \otimes u) + \nabla p - \frac{1}{Re}\Delta u = 0\,. \tag{9}$$

In Eulerian approach, the velocities are defined regarding fixed computational mesh. This description requires accurate definition of boundaries, but allows precise calculation of large distortions in fluid motion. Cases with moving boundaries can be solved with

ALE approach in which nodes of fluid mesh can move independently of the fluid particles. This formulation factors the velocity of boundaries and the fluid mesh u_g in NS equation:

$$\dot{u} + \nabla \cdot \left((u - u_g) \otimes u \right) + \nabla p - \frac{1}{Re} \Delta u = 0 \qquad (10)$$

where $\boldsymbol{c} = u - u_g$ is a relative velocity between the material and the mesh. In this formulation, mesh acceleration can be neglected [15,16].

3. Simulation model

To simplify three dimensional phenomena, two dimensional model was used. The *plane strain* approximation was used for this model. The displacements in axis perpendicular to selected cross-section plane are assumed to be zero. In that case, a normal stress exists in addition to the other stress components. This approach is applied for long bodies with constant cross-sectional area and when external forces are not acting along perpendicular axis. The main disadvantage of this approximation is neglecting stresses and strains near the ends of the structure (in perpendicular direction), but computations for middle part of object are comparable to three dimensional calculations and exact solution.

The simulation model consists of an elastic body submerged in fluid. The dimensions are based on the benchmark model proposed in [13] and [14]. The origin is assumed at the bottom-left corner of the domain. The channel (fluid domain) is 2.5 meters long and 0.41 meters high. The solid domain has two parts. One of them is a fixed circular structure (white object in Fig. 1) with a center at point (0.2 m, 0.2 m). We assume no deformations of this object. The elastic plate is another part of the solid domain. Its dimensions are shown in figure 2 (structure marked with grey color). The total length of the elastic object is equal to 0.35 meters and thickness is 0.02 m. As mentioned earlier, plane strain approximation was used. Therefore, the dimension in perpendicular axis was necessary to define and value of 1 m were chosen, according to benchmark model [13].
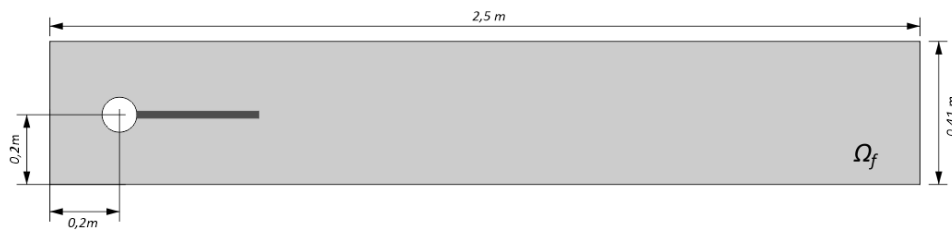

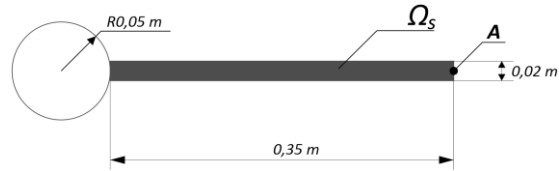Figure 1. Dimensions of the computation domain

Figure 2. Dimensions of solid domain

The circular object is positioned with a small offset from the symmetry axis of the channel. The reason for such offset is to avoid dependence of the onset of possible oscillations on the precision of the computation and to maintain consent with the benchmarking model [13].

3.1. Properties of materials

The properties of the fluid and elastic solid are presented in table 1.

Table 1. The properties of fluid and solid

Quantity	Symbol	Unit	Value
Fluid density	ρ_f	kg/m^3	1250
Dynamic viscosity	ν_d	Pa s	1
Young's modulus	E	MPa	5.6
Solid density	ρ_s	kg/m^3	1150

The materials are assumed to be similar to glycerin and highly elastic polyurethane. One more value is needed to fully define solid material properties – Poisson's ratio. This value is changed in each simulation and is in the range from -0.95 to 0.45 with a step of 0.05. Such changes allow observing differences in deformations induced by fluid flow.

3.2. Boundary conditions

The inflow condition is applied to the left boundary of the channel. The velocity value is chosen based on equation (7). The laminar regime of flow is required to observe formation on von Karman vortexes, which interacts with structure and causes deformations. Additionally, the fluid should have a high viscosity (i.e. glycerin). The characteristic dimension in this simulation (used in equation (7)) is the radius of the circular shape. Reynold's number in such simulation should be slightly higher than the upper threshold value for von Kármán vortex street (Re = 140 – 160). The velocity U is calculated for a value of 200. The fully developed inlet velocity profile is assumed with a mean value of $U = 2$ m/s. It is defined as:

$$u_f(0, y) = 1.5U \frac{y(H-y)}{\left(\frac{H}{2}\right)^2} \theta(t), \qquad (9)$$

where *y* is the position concerning the origin, *H* is the height of the channel (0.41 m) and θ is the function shown in figure 3. This function is used to initialize and develop flow in the first second of the simulation.
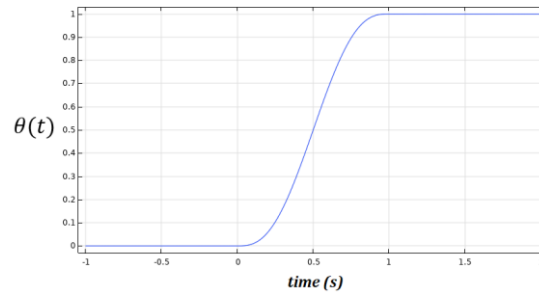

Figure 3. Values of function $\theta(t)$

The outflow boundary is assumed to be one on the right side of the channel. In our simulation, the pressure at outflow was assumed to be 0 and no backflow was allowed. On boundary $\Gamma_0(t)$, the no-slip condition was applied.

3.3. Mesh and simulation settings

The simulations were conducted in Comsol Multiphysics. The mesh is divided into three parts as shown in figure 4. The mesh consists of 5372 elements (3890 triangle elements and 1482 quad elements). The minimum element quality is 0.3814 and the average element quality is equal to 0.9056.
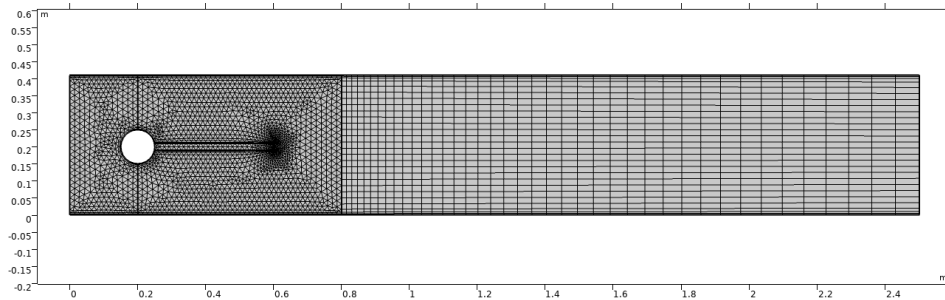

Figure 4. Mesh used for finite element method

The most left part of the mesh is the region, where flow around circular objects can be observed and the velocity profile is shaped. In the middle part, the mesh is finer and refined around the end of the plate (point A in figure 2). It was necessary to obtain a proper mapping of moving mesh in a fully implicit ALE formulation of mesh deformation. The

most right part is less refined and more coarse. Additional boundary layers were added around an obstacle and at both horizontal channel walls.

The simulation time is in the range from 0 to 5 seconds, as for all values of Poisson's ratio at least one full period of vibration was observed. The time-step is dynamic, and output values are taken in 0.05 s intervals.

4. Results

The displacements in the X and Y axis of point A (Fig. 2) for different values of Poisson's ratio are shown in figures 5–9.
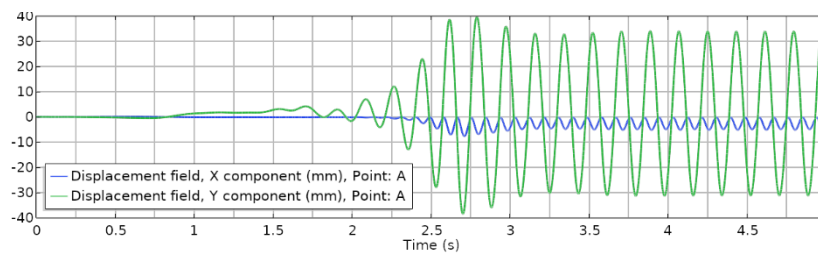

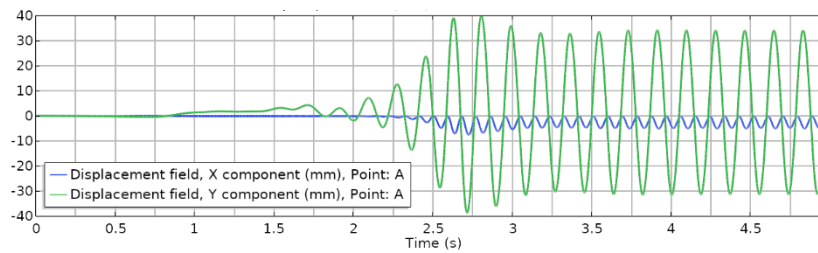Figure 5. Point A displacement, Poisson's ratio: 0.45

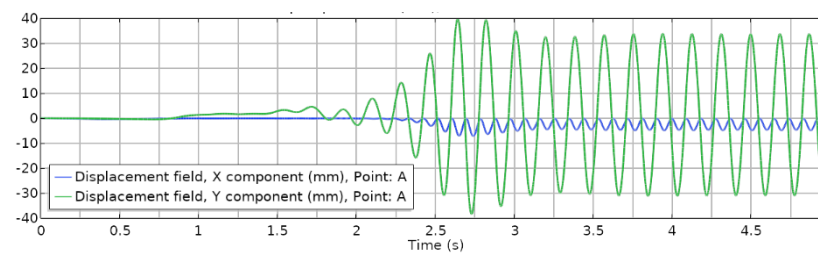Figure 6. Point A displacement, Poisson's ratio: 0.35

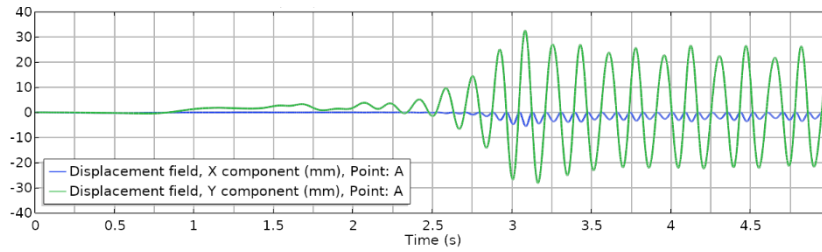Figure 7. Point A displacement, Poisson's ratio: 0.0

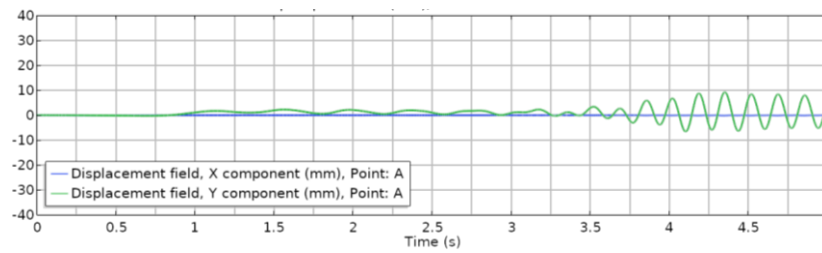Figure 8. Point A displacement, Poisson's ratio: -0.75

Figure 9. Point A displacement, Poisson's ratio: -0.95

Figure 10 shows deformations, velocity field, and the von Mises stress in the deformed structure for Poisson's ratio $\nu = 0.35$. Deformed von Kármán vortex street can be observed past the structure and they also affect the flow.
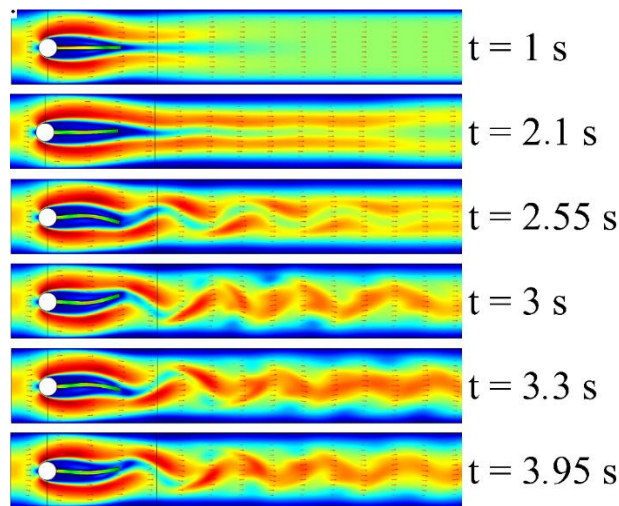

Figure 10. Deformations, velocity field, and the von Mises stress in deformed structure for Poisson's ratio $\nu = 0.35$ in different timeframes.

The computed values for other Poisson's ratios are shown in table 2. All values in tables were rounded to 0.01.

Table 2. The displacement of point A for different Poisson's ratios

Poisson's ratio	Absolute maximum displacement in X-axis [mm]	Absolute maximum displacement in Y-axis [mm]	The maximum peak-to-peak value of displacement in X-axis [mm]	The maximum peak-to-peak value of displacement in Y-axis [mm]	The absolute peak value of displacement in X-axis during fully developed periodic vibrations [mm]	The absolute peak value of displacement in Y-axis during fully developed periodic vibrations [mm]	Dominant vibration's frequency with Y-axis [Hz]
-0.95	0.17	9.30	0.10	15.70	0.07	13.20	6.00
-0.85	1.90	18.80	1.90	35.90	1.30	17.10	5.80
-0.75	5.50	32.60	5.60	60.70	3.50	26.30	5.80
-0.65	7.10	37.70	7.00	72.50	4.60	31.10	5.70
-0.55	7.45	40.00	7.45	76.50	4.90	32.80	5.60
-0.45	7.45	40.75	7.45	77.65	4.97	33.20	5.60
-0.35	7.30	40.75	7.35	77.80	4.95	33.65	5.40
-0.25	7.34	40.50	7.39	78.30	4.93	33.75	5.40
-0.15	7.35	40.47	7.40	78.47	4.86	33.75	5.40
-0.1	7.35	40.50	7.40	78.50	4.86	33.65	5.40
0	7.10	39.80	7.00	78.20	4.80	33.80	5.40
0.1	7.20	40.05	7.10	78.55	4.90	33.82	5.40
0.15	7.43	40.20	7.38	78.80	4.95	33.85	5.40
0.25	7.52	40.22	7.47	78.92	5.02	34.05	5.40
0.35	7.60	39.94	7.53	78.69	5.10	34.08	5.40
0.4	7.65	40.85	7.63	78.79	5.13	34.11	5.38
0.45	7.67	39.63	7.60	78.14	5.15	33.92	5.50

5. Conclusions

Presented results of numerical simulation show dependence between Poisson's ratio of material and deformations of the structure. The lowest value of displacement can be observed for small values of Poisson's ratio – values near -1. For those parameters. vibrations induced by fluid flow have a slightly higher frequency (about 6.0 Hz). Also. periodic oscillations appear after a long time (after about 4 s) than for higher values of Poisson's ratio.

Obtained results clearly show that auxetic structures can successfully decrease vibrations in objects exposed to fluid flow around them. The main area of application in engineering would be creating airplane wings or rotors with such structure to limit the negative effects of vibrations, such as fatigue wear and dynamic loads in these machines. In some cases. replacing conventional materials with auxetics can change the frequency of vibrations.

Acknowledgments

References

1. H. Lamb, *On the vibrations of an elastic plate in contact with water*. Proc Royal Soc London. Ser A Nov.. 98 (1920) 205-216.
2. B. Gjerek. R. Drazumeric. F. Kosel. *Flutter behavior of a flexible airfoil: Multiparameter experimental study*. Aerospace Science and Technology, 36 (2014) 75-86.
3. Y.W. Kwon, E.M Priest. J.H. Gordis. *Investigation of vibrational characteristics of composite beams with fluid-structure interactio*n, Composite Structures. 105 (2013) 269-278.
4. T. Strek. *Forced Response of Plate with Viscoelastic Auxetic Dampers*, Vibrations in Physical Systems. 29 (2018) 2018003.
5. W. Wu, W. Hu, G. Qian, H. Liao, X. Xu, F. Berto, *Mechanical design and multifunctional applications of chiral mechanical metamaterials: A review,* Materials & Design. 180 (2019) 107950.
6. R. Lakes. *Foam structures with a negative Poisson's ratio*, Science, 235 (1987) 1038–1040.
7. Y. Li, C. Zeng, *On the successful fabrication of auxetic polyurethane foams: Materials requirement. processing strategy and conversion mechanism*, Polymer, 87 (2016) 98–107.
8. T. Strek, J. Michalski, H. Jopek. *Computational Analysis of the Mechanical Impedance of the Sandwich Beam with Auxetic Metal Foam Core*, Physica Status Solidi B, 256 (2018) 1800423.
9. F. Scarpa, *Damping in auxetic materials and structures,* The Journal of the Acoustical Society of America. 127 (2010) 1888.

10. A. Matuszewska, T. Strek, *Vibration properties of auxetic beam*. Vibrations in Physical Systems, 29 (2018) 2018031.
11. E. Idczak, T. Strek, *Computational Modelling of Vibrations Transmission Loss of Auxetic Lattice Structure*, Vibrations in Physical Systems, 27 (2016) 123–128.
12. S. Turek, J. Hron, *Proposal for Numerical Benchmarking of Fluid-Structure Interaction Between an Elastic Object and Laminar Incompressible Flow*, Fluid-Structure Interaction Lecture Notes in Computational Science and Engineering 53 (2006) 246–260.
13. S. Turek, M. Schäfer, *Benchmark computations of laminar flow around cylinder*. Flow Simulation with High-Performance Computers II. Notes on Numerical Fluid Mechanics, 52 (1996) 547–566.
14. O.C. Zienkiewicz, R.L. Taylor, *The Finite Element Method: Fluid Dynamics,* Butterworth-Heinemann 2014.
15. W. Stankiewicz, R. Roszak, M. Morzyński, *Arbitrary Lagrangian-Eulerian approach in reduced order modeling of a flow with a moving boundary,* Progress in Flight Physics 5 (2013) 109-124
16. G. Fu, *Arbitrary Lagrangian–Eulerian hybridizable discontinuous Galerkin methods for incompressible flow with moving boundaries and interfaces,* Computer Methods in Applied Mechanics and Engineering, 367 (2020) 113158.